Research on Distributed Coordination Control Method for Microgrid System Based on Finite-time Event-triggered Consensus Algorithm*

Lizhen Wu[1, 2], *Heng Yang*[1], *Jianping Wei*[1] *and Wendong Jiang*[1]
(1. College of Electrical and Information Engineering,
Lanzhou University of Technology, Lanzhou 730050, China;
2. National Active Distribution Network Technology Research Center,
Beijing Jiaotong University, Beijing 100044, China)

Abstract: Microgrids are networked control systems with multiple distributed generators (DGs). Microgrids are associated with many problems, such as communication delays, high sampling rates, and frequent controller updates, which make it challenging to realize coordination control among the DGs. Therefore, finite-time consensus algorithms and event-triggered control methods are combined to propose a distributed coordination control method for microgrid systems. The DG in the microgrid system serves as an agent node in the control network, and a distributed secondary controller is designed using finite-time consensus algorithm, such that the frequency and voltage restoration control has a faster convergence time and better anti-interference performance. The event-triggered function was designed based on the state information of the agents. The controller exchanges the state information at the trigger instants. System stability is analyzed using the Lyapunov stability theory, and it is verified that the controller cannot exhibit the Zeno phenomenon in the event-triggered process. A simulation platform was developed in Matlab/Simulink to verify that the proposed control method can effectively reduce the frequency of controller updates during communication delays and the burden on the communication network.

Keywords: Microgrid, event-triggered control, distributed secondary control, finite-time consensus algorithm, coordination control

1 Introduction

With the rapid expansion of renewable energy power generation, centralized renewable energy power generation systems face challenges in safe and stable system operation, long-distance transmission, energy consumption, etc. [1] The distributed generation (DG) can be connected to the distribution network to realize local consumption, thus, it has been vigorously developed. However, DG changes the structure of the distribution network, affects the power quality of the distribution network, and makes it difficult to ensure the safe operation and coordination control of the distribution network. A microgrid is a bridge and link for distributed power sources to connect to a distribution network, providing an effective method for renewable energy consumption [2-4].

In a microgrid system, droop control cannot achieve power sharing in proportion to the capacity of DGs. Many improved droop control methods have been proposed to improve the accuracy of reactive power sharing. However, the characteristics of the droop control method vary, and most schemes are complicated and challenging to implement in engineering practice. Guerrero et al. [5] proposed a hierarchical control structure to achieve voltage deviation regulation and reactive power equalization control using a secondary control method. Although the regulation accuracy of the centralized secondary control method is high, the existence of a central node reduces the reliability of the system and requires a high communication bandwidth [6]. The distributed secondary control method overcomes the shortcomings of centralized secondary control; it does not have a central node, and has high reliability and

Manuscript received September 2, 2023; revised October 19, 2023; accepted December 17, 2023. Date of publication June 30, 2024; date of current version December 21, 2023.
* Corresponding Author, E-mail: wulzlut@163.com
* Supported by the National Natural Science Foundation of China (62063016).
Digital Object Identifier: 10.23919/CJEE.2024.000053

scalability for system control [7-8]. Bidram et al. [9] introduced a distributed control method based on a multi-agent system (MAS) for the secondary control of a microgrid. The distributed secondary control method based on a consensus algorithm is used to adjust the voltage and current consensus of the microgrid, achieving 'plug and play' and reducing dependence on the communication network, obtaining good control results [10]. However, the distributed secondary control method based on the consensus algorithm is a time-triggered control method that uses a cyclic communication method and communicates more frequently, thereby increasing the communication burden. An event-triggered control method has been proposed for a multi-agent system. Non-cyclic communication can reduce the communication burden between the controller and actuator and improve the efficiency of the entire system. Ref. [11] investigated cyclic event driving using a quadratic Lyapunov function to design an event-triggered scheme for the consensus problem of fixed or switched undirected connected network topologies.

However, continuous agent communication is required, which requires a high network bandwidth. By combining an adaptive control protocol with an event-triggered communication method, an event-triggered control method based on adaptive control was proposed, which enables the agents to update the state only when the event is triggered without requiring global parameters [12]. In recent years, event-triggered control methods have been applied to microgrid coordination control to reduce the communication burden on microgrid systems. An adaptive event-triggered secondary control method has been proposed to achieve voltage regulation and proportional load power sharing [13-14]. However, it requires the application of current and voltage estimators to generate event-triggered conditions, which are complex and challenging to apply in engineering. A discrete-time event-triggered control method was proposed for bus voltage and current-sharing control in microgrids. Nevertheless, the Laplace matrices of electrical and communication networks are assumed interchangeable, limiting their flexibility and scalability [15]. Ref. [16] introduces an event-triggered distributed active power distribution control for microgrids based on droop control; however, it adopted cyclical sampling of the event-triggered condition without considering the communication burden. In Ref. [17], an event-triggered distributed control method with asynchronous sampling for frequency and voltage control, with full consideration of the communication burden, was proposed to achieve accurate active power sharing. Abdolmaleki et al. [18] added an event-triggered approach to the leader-follower tracking control method to implement inverter-based microgrid voltage control; however, the leader needs to generate reference values and does not consider the effect of communication delay. In Refs. [19-20], the authors developed an event-triggering mechanism based on discrete sampling data for the distributed secondary control of islanded microgrids to achieve frequency restoration control and accurate power sharing while avoiding the Zeno phenomenon.

The event-triggered control method effectively reduces the sampling rate of the controller and the bandwidth requirement of the system. However, the convergence speed of the system must be faster to operate stably in a finite time. Finite-time consensus control has a fast convergence rate that can achieve convergence within finite time and optimal control in time optimization. They also exhibit good robustness and adapt to various uncertain disturbances [21-23]. The advantages of the finite-time consensus control can be applied to practical microgrid systems.

To this end, a microgrid secondary control method based on finite-time consensus was proposed for designing frequency-active and voltage-reactive power controllers [24]. The proposed control schemes improve the power-sharing accuracy while achieving frequency and voltage static adjustments within a finite time. Recently, a robust finite-time control algorithm was established for the secondary coordination control of islanded microgrids that maintained the convergence of the system even under parameter perturbations and various disturbances [25]. A finite-time quadratic control method with bounded control inputs was proposed to solve the problems of frequency restoration control and accurate active power sharing, suppressing sudden changes in transient processes [26]. In Ref. [27], the authors developed a robust distributed

secondary control scheme under a directed communication graph to restore the frequency to the nominal value and achieve accurate active power sharing in finite time. In Ref. [28], finite-time event-triggered secondary control for islanded DC microgrids was introduced to achieve accurate power sharing and voltage restoration in finite time while reducing the burden on the communication network.

Therefore, this paper proposes a finite-time event-triggered consensus distributed coordination control method for microgrids. The finite-time consensus algorithm is applied to design distributed secondary controllers for distributed power sources in microgrid systems. The DG serves as an agent, the event-trigger function is designed according to the state information of the agents, and the controller is designed using a finite-time consensus algorithm. The stability of the control system is analyzed using the Lyapunov stability theory, and the Zeno phenomenon is analyzed. Finally, the dynamic performance of the proposed method is verified.

2 Preliminaries

2.1 Distributed coordination control architecture of microgrid system

A microgrid-distributed hierarchical control architecture based on the finite-time event-triggered consensus algorithm is shown in Fig. 1. The hierarchical control structure is primarily composed of a primary control layer and a secondary control layer based on event triggered method.

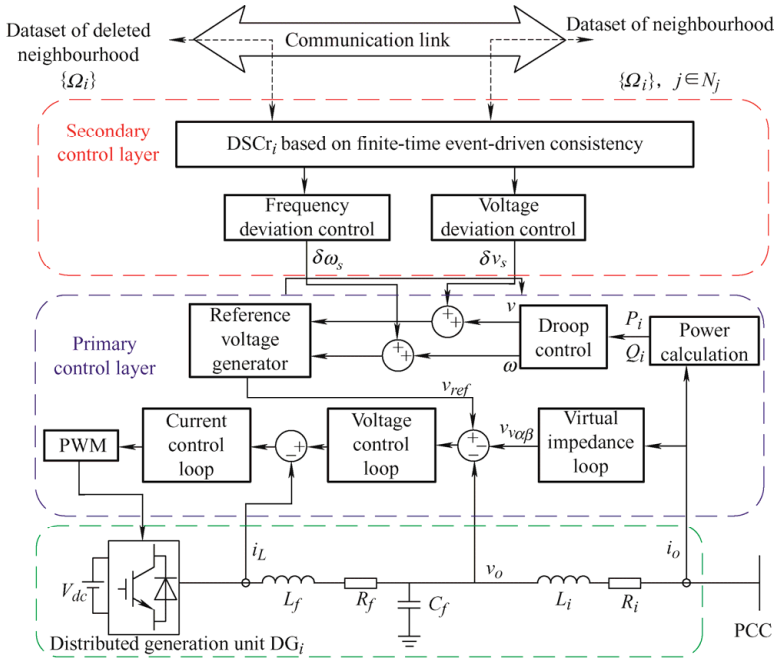

Fig. 1 Microgrid event-triggered consensus hierarchical control block diagram

In the primary control layer of a microgrid, droop control is typically used to achieve system stability, which is described as follows

$$\begin{cases} \omega_i = \omega_0 - K_p P_i + \delta\omega_s \\ v_i = v_0 - K_q Q_i + \delta v_s \end{cases} \tag{1}$$

where ω_i and v_i denote the output angular frequency and voltage amplitude of the DG, respectively; ω_0 and v_0 denote the reference value for the angular frequency and voltage amplitude of the DG output, respectively. P_i and Q_i represent the active and reactive powers, respectively.

In the secondary control layer, each DG acts as an agent node of the networked control system, with a DSCr (distributed secondary controller) equipped with a communication interface to realize information interaction between the controllers. A finite-time event-triggered consensus algorithm is embedded into each DSCr; thus, each DSCr has consensus estimation and communication functions. From Fig. 1, when an event is triggered, DSCr_i collects the state information of DG_i and sends it to neighbor DSCr_j, while receiving the state information of DSCr_j. The voltage and frequency deviations were adjusted using DSCr.

2.2 Finite-time event-triggered consensus algorithm

The frequency and active power restoration times T_f and T_p ensure that each DG droop control ω_{ref} satisfies the relationships expressed in Eqs. (2) and (3)

$$\begin{cases}\lim\limits_{t\to T_f}[\omega_i(t)-\omega_j(t)]=0\\ \omega_i(t)=\omega_j(t)=\omega_{ref}\end{cases} \quad t\geqslant T_f, i,j\in\{1,2,\cdots,N\} \tag{2}$$

$$\begin{cases}\lim\limits_{t\to T_p}[K_{pi}P_i-K_{pj}P_j]=0\\ K_{pi}P_i=K_{pj}P_j\end{cases} \quad t\geqslant T_p, i,j\in\{1,2,\cdots,N\} \tag{3}$$

The restoration time for frequency and active power sharing is

$$T_F=\max\{T_f,T_p\} \tag{4}$$

The voltage restoration time T_v enables each DG droop control v_{ref} to satisfy the relationships described in Eq. (5).

$$\begin{cases}\lim\limits_{t\to T_v}[v_i(t)-v_j(t)]=0\\ v_i(t)=v_j(t)=v_{ref}\end{cases} \quad t\geqslant T_v, i,j\in\{1,2,\cdots,N\} \tag{5}$$

The event-triggered control method has the advantages of reducing the number of controller updates and communication burden, making it widely used in resource-constrained environments. The event-triggered control method is integrated with a finite-time event-triggered consensus algorithm to form an event-triggered consensus control method. This method primarily involves graph theory, which is briefly described as follows.

Let the communication topology of an microgrid system be inscribed by $G=(V,E,\boldsymbol{A})$; where $V=\{1,2,\cdots,N\}$ is the set of nodes, $E\in V\times V$ is the set of edges, and $\boldsymbol{A}=[a_{ij}]\in\boldsymbol{R}^{N\times N}$ represents the adjacency matrix.

The Laplace matrix of the weighted graph G is defined as $\boldsymbol{L}=\boldsymbol{D}-\boldsymbol{A}$; where $\boldsymbol{D}=\{d_i,\cdots,d_N\}$ represents the degree matrix, and $d_i=\sum\limits_{j\in N_i}a_{ij}$ [29].

For a multi-agent system composed of continuous first-order integrators, the dynamic equation of each agent can be described as

$$\dot{x}_i(t)=u_i(t) \qquad i\in 1,2,\cdots,N \tag{6}$$

where N indicates the number of smart nodes, x_i indicates the state variable of the smart node i (the variable can be the actual physical quantity of the system, such as power, voltage, and current), and u_i represents the control input of the smart node i.

Each node can communicate only with its neighbors and exchange status information. The communication topology between nodes is represented by an undirected graph G. For any intelligent node $i\in V$, its latest transmission information of intelligent node i is

$$\hat{x}_i(t)=x_i(t_k^i) \qquad t\in[t_k^i,t_{k+1}^i] \tag{7}$$

where $\{t_k^i,k=0,1,\cdots\}$ denotes the sequence of message broadcast moments of smart node i. In asynchronous event-triggered control mechanisms, the event-triggered conditions can be described as follows

$$t_{k+1}^i=\inf\left\{t>t_k^i\,|\,f_i(t)\geqslant 0\right\} \tag{8}$$

$$f_i(t)=E(t)-ky(t) \tag{9}$$

where $E(t)$ represents the difference term; k is the threshold coefficient; and $k>0$, $y(t)$ is the threshold term.

Using Lyapunov stability theory, a finite-time consensus algorithm of the following form is obtained

$$u_i(t)=-\beta sign\left\{\left[\sum_{j\in N_i}a_{ij}(x_i-x_j)+b_i(x_i-x_{ref})\right]^{\alpha}\right\} \tag{10}$$

where, α and β are finite-time control parameters, α is an exponential coefficient and $0<\alpha<1$, which makes a fractional power term in the consensus algorithm and improves the convergence performance; β is a scale factor and $\beta>0$,which determines the step size of the control variable; a_{ij}, b_i are the adjacency coefficient, when a communication link exists between agents i and j, $a_{ij}\geqslant 0$, $b_i\geqslant 0$, otherwise, $a_{ij}=0$, $b_i=0$; $sign$ represents the sign function, defined as follows

$$sign(x)=\begin{cases}1 & x>0\\ 0 & x=0\\ -1 & x<0\end{cases} \tag{11}$$

2.3 Convergence proof

To use Lyapunov stability theory to investigate the stability of the system, the following Lyapunov function is constructed

$$V(t)=V_\omega+V_p \tag{12}$$

$$V_\omega=\sum_{i=1}^{n}\frac{\beta_{\omega i}}{1+\alpha_{\omega i}}\left|y_{\omega i}\right|^{1+\alpha_{\omega i}} \tag{13}$$

Clearly, $V_\omega > 0$, the derivative of Eq. (13) can be expressed as follows

$$\dot{V}_\omega = \sum_{i=1}^{n} \frac{\beta_{\omega i}}{1+\alpha_{\omega i}}(1+\alpha_{\omega i}) sign\left\{ |y_{\omega i}|^{\alpha_{\omega i}} \right\} =$$
$$\sum_{i=1}^{n} \beta_{\omega i} sign\left\{ (y_i)^{\alpha_{\omega i}} \right\} \left[-L_i \left(I_n \otimes \beta_\omega \right) sign\left\{ (y_\omega + E_\omega)^{\alpha_{\omega i}} \right\} \right] =$$
$$-\sum_{i=1}^{n} \beta_{\omega i} sign\left\{ (y_i)^{\alpha_{\omega i}} \right\} \left\{ \sum_{j=1}^{n} \beta_{\omega j} l_{ij} sign\left\{ (y_{\omega j} + E_{\omega j})^{\alpha_{\omega j}} \right\} \right\} =$$
$$-\sum_{i=1}^{n}\sum_{j=1}^{n} \left\{ \beta_{\omega i} sign\left\{ (y_{\omega i})^{\alpha_{\omega i}} \right\} \right\} l_{ij} \left\{ \beta_{\omega j} sign\left\{ (y_{\omega j} + E_{\omega j})^{\alpha_{\omega j}} \right\} \right\} =$$
$$-\sum_{i=1}^{n}\sum_{j\in N_i}^{n} \left\{ \beta_{\omega i} sign\left\{ (y_{\omega i})^{\alpha_{\omega i}} \right\} \right\} l_{ij} \left\{ \beta_{\omega j} sign\left\{ (y_{\omega j} + E_{\omega j})^{\alpha_{\omega j}} \right\} \right\} \tag{14}$$

where $L_i = [l_{i1}, l_{i2}, \cdots, l_{in}]$, $y_\omega = [y_{\omega 1}, \cdots, y_{\omega i}, \cdots, y_{\omega j}, \cdots]$, $E_\omega = [E_{\omega 1}, \cdots, E_{\omega i}, \cdots, E_{\omega j}, \cdots]$. Subsequently, the following equation is derived

$$sign\left\{ (y_{\omega i})^{\alpha_{\omega i}} \right\} \leqslant |y_{\omega i}|^{\alpha_{\omega i}} \tag{15}$$

$$sign\left\{ (y_{\omega i})^{\alpha_{\omega i}} \right\} (y_{\omega j} + E_{\omega j})^{\alpha_{\omega j}} \leqslant |y_{\omega j} + E_{\omega j}|^{\alpha_{\omega j}} \leqslant$$
$$\left(|y_{\omega j}| + |E_{\omega j}| \right)^{\alpha_{\omega j}} \leqslant |y_{\omega j}|^{\alpha_{\omega j}} + |E_{\omega j}|^{\alpha_{\omega j}} \tag{16}$$

Combining Eqs. (15) and (16), Eq. (14) can be rewritten as follows

$$\sum_{i=0}^{n}\sum_{j\in N_i}^{n} \left\{ \left\{ \beta_{\omega i} sign\left\{ (y_{\omega i})^{\alpha_{\omega i}} \right\} \right\} l_{ij} \left\{ \beta_{\omega j} sign\left\{ (y_{\omega i} + E_{\omega j})^{\alpha_{\omega i}} \right\} \right\} \right\} \geqslant$$
$$\sum_{i=0}^{n}\sum_{j\in N_i}^{n} \left\{ \left(\beta_{\omega i} |y_{\omega i}|^{\alpha_{\omega i}} \right) l_{ij} \left[\beta_{\omega j} \left(|y_{\omega j}|^{\alpha_{\omega j}} + |E_{\omega j}|^{\alpha_{\omega j}} \right) \right] \right\} \tag{17}$$

Furthermore, $\mathrm{d}V_\omega / \mathrm{d}t$ can be written as

$$\dot{V}_\omega \leqslant -\sum_{i=1}^{n}\sum_{j\in N_i}^{n} \left(\beta_{\omega i} |y_{\omega i}|^{\alpha_{\omega i}} \right) l_{ij} \left[\beta_{\omega j} \left(|y_{\omega j}|^{\alpha_{\omega j}} + |E_{\omega j}|^{\alpha_{\omega j}} \right) \right] \leqslant$$
$$-\sum_{i=1}^{n}\sum_{j\in N_i}^{n} \left(\beta_{\omega i} |y_{\omega i}|^{\alpha_{\omega i}} \right) l_{ij} \left[\beta_{\omega j} \left(1 + k_{\omega j}{}^{\alpha_{\omega i}} \right) |y_{\omega j}|^{\alpha_{\omega j}} \right] \leqslant$$
$$-\left(\beta_{\omega i} |y_{\omega i}|^{\alpha_{\omega i}} \right)^{\mathrm{T}} L \left(1 + K_\omega \right) \left(\beta_{\omega j} |y_{\omega j}|^{\alpha_{\omega j}} \right) \tag{18}$$

where $K_\omega = \left[k_{\omega 1}{}^{\alpha_{\omega 1}}, \cdots, k_{\omega N}{}^{\alpha_{\omega N}} \right]$.

Let $\boldsymbol{M} = \boldsymbol{L}\left(1 + K_\omega \right)$, $\boldsymbol{P} = \frac{1}{2}\left(\boldsymbol{M} + \boldsymbol{M}^{\mathrm{T}} \right)$ and $\boldsymbol{\Lambda} = \{ \boldsymbol{\delta} \in \boldsymbol{R} : \boldsymbol{\delta}^{\mathrm{T}} \boldsymbol{\delta} = 1 \cap \boldsymbol{\delta} = \beta_\omega |\boldsymbol{\zeta}|^{\alpha_\omega}, \boldsymbol{\zeta} \perp 1 \}$, then

$$\frac{(\beta_\omega |y_\omega|^{\alpha_\omega})^{\mathrm{T}} \boldsymbol{M} (\beta_\omega |y_\omega|^{\alpha_\omega})}{(\beta_\omega |y_\omega|^{\alpha_\omega})^{\mathrm{T}} (\beta_\omega |y_\omega|^{\alpha_\omega})} \geqslant \min_{\boldsymbol{\delta}\in\boldsymbol{\Lambda}} \boldsymbol{\delta}^{\mathrm{T}} \boldsymbol{P} \boldsymbol{\delta} \tag{19}$$

Define $\Xi = \dfrac{\dot{V}_\omega}{V_\omega(t)^{\frac{2\alpha_\omega}{1+\alpha_\omega}}}$, then

$$\Xi \geqslant \frac{k_\omega (\beta_\omega |y_\omega|^{\alpha_\omega})^{\mathrm{T}} (\beta_\omega |y_\omega|^{\alpha_\omega})}{V_\omega(t)^{\frac{2\alpha_\omega}{1+\alpha_\omega}}} \geqslant \frac{k_\omega (\beta_\omega |y_\omega|^{\alpha_\omega})^{\mathrm{T}} (\beta_\omega |y_\omega|^{\alpha_\omega})}{\sum_{i=1}^{n} \left(\frac{\beta_{\omega i}}{1+\alpha_{\omega i}} |y_{\omega i}|^{1+\alpha_{\omega i}} \right)^{\frac{2\alpha_{\omega i}}{1+\alpha_{\omega i}}}} \geqslant$$
$$\frac{k_\omega \sum_{i=1}^{n} \beta_{\omega i}{}^2 |y_{\omega i}|^{2\alpha_{\omega i}}}{\sum_{i=1}^{n} \left(\frac{\beta_{\omega i}}{1+\alpha_{\omega i}} |y_{\omega i}|^{1+\alpha_{\omega i}} \right)^{\frac{2\alpha_{\omega i}}{1+\alpha_{\omega i}}}} \tag{20}$$

Let $k' = \dfrac{k'_\omega \|\beta_\omega\|^2}{\left(\frac{\|\beta_\omega\|}{1+\|\alpha_\omega\|} \right)^{\frac{2\|\alpha_{\omega i}\|}{1+\|\alpha_{\omega i}\|}}}$, then the derivative of the Lyapunov function is upper bounded by

$$\dot{V}_\omega \leqslant -k'_\omega V_\omega(t)^{\frac{2\alpha_\omega}{1+\alpha_\omega}} \tag{21}$$

2.4 Analysis of Zeno phenomenon

The Zeno phenomenon refers to infinite sampling within finite time. The Zeno phenomenon not only violates the purpose of reducing communication bandwidth and other resources, but also tends to cause disorder in the system, which is not allowed in practical applications. Whether the Zeno phenomenon can be effectively avoided in an event-triggered mechanism depends on whether the event conditions are reasonably designed. The design of the event-triggered function must satisfy stability and feasibility requirements. Stability refers to the achievement of a control objective without disturbing the steady-state operation of the microgrid. Feasibility refers to communication when an event-triggered condition is obtained, which must ensure the existence of a positive lower bound at adjacent sampling intervals.

A lower event-bound t_D exists between any k-th event-triggered time t_k

$$t_{k+1} - t_k \geqslant t_D > 0 \tag{22}$$

Eqs. (2)-(5) indicate that the designed control method enables the system to achieve restoration control within a finite time, and Eq. (22) indicates that the event-triggered method can avoid infinite triggered events within a finite time.

3 Controller design

The key to event-triggered control is the design of the

triggering conditions, which can be described using mathematical expressions related to the system state and measurement output. The voltage and frequency event-triggered consensus control conditions are detailed in the following subsection.

3.1 Frequency secondary controller design

A distributed secondary controller (DSCr) based on a finite-time event-triggered consensus algorithm is designed for frequency and active power sharing to restore the output frequency of each DG to its rated value. By applying the input-output feedback linearization method, the dynamic system equation is obtained by differentiating Eq. (1).

$$\begin{cases} \dot{\omega}_i(t) = \dot{\omega}_0 - K_{Pi}\dot{P}_i = u_{\omega i}(t) \\ K_{Pi}\dot{P}_i = u_{Pi}(t) \end{cases} \tag{23}$$

where $u_{\omega i}$, u_{Pi} represent the frequency and active power secondary controllers of DG_i, respectively.

According to the finite-time consensus algorithm shown in Eq. (10), the secondary controllers, $u_{\omega i}$ and u_{Pi}, for controlling the input are designed as follows

$$\begin{cases} u_{\omega i} = -\beta_{\omega i} sign\left\{ \left[\sum_{j\in N_i} a_{ij}\left(\omega_i - \omega_j\right) + b_i\left(\omega_i - \omega_{ref}\right) \right]^{\alpha_{\omega i}} \right\} \\ u_{Pi} = -\beta_{Pi} sign\left\{ \left[\sum_{j\in N_i} a_{ij}\left(K_{Pi}P_i - K_{Pj}P_j\right) \right]^{\alpha_{Pi}} \right\} \end{cases} \tag{24}$$

where $\alpha_{\omega i}$ and α_{Pi} represent the frequency control gain and active power control gain of DG_i, respectively; $\alpha_{\omega i} \in (0,1)$, $\alpha_{Pi} \in (0,1)$, $\beta_{\omega i}$, and β_{Pi} are the proportion coefficients of the frequency and active power, respectively; $\beta_{\omega i} > 0$, $\beta_{Pi} > 0$, $sign(\cdot)$ is signed function and $sign\{\cdot\} = sign(\cdot)|\cdot|$.

A distributed controller constructed based on the finite-time consensus algorithm requires continuous state feedback, which increases the communication burden of the agents. An event-triggered method is adopted to reduce the dependence of the DG on communication networks, and Eq. (24) can be transformed into Eq. (25) and is expressed as

$$\begin{cases} u_{\omega i} = -\beta_{\omega i} sign\left\{ \left[\sum_{j\in N_i} a_{ij}\left(\hat{\omega}_i - \hat{\omega}_j\right) + b_i\left(\hat{\omega}_i - \omega_{ref}\right) \right]^{\alpha_{\omega i}} \right\} \\ u_{Pi} = -\beta_{Pi} sign\left\{ \left[\sum_{j\in N_i} a_{ij}\left(K_{Pi}\hat{P}_i - K_{Pj}\hat{P}_j\right) \right]^{\alpha_{Pi}} \right\} \end{cases} \tag{25}$$

where the label ^ denotes the observed value of the corresponding variable, expressed as follows

$$\begin{cases} \hat{\omega}_i(t) = \omega_i(t_{l_{wi}}) \\ K_{Pi}\hat{P}_i(t) = K_{Pi}P_i(t_{l_{Pi}}) \end{cases} \tag{26}$$

where $l_{\omega i}$ and l_{Pi} represent the l-th event-triggered of the frequency controller and active power controller of DG_i, respectively. To determine the event-triggered time, the frequency observation error $e_{wi}(t)$ and the active power observation error $e_{Pi}(t)$ are defined as follows

$$\begin{cases} e_{\omega i}(t) = \omega_i(t_{l_{wi}}) - \omega_i(t) \\ e_{Pi}(t) = K_{Pi}P_i(t_{l_{Pi}}) - K_{Pi}P_i(t) \end{cases} \tag{27}$$

The process of generating event-triggered times is depicted in Fig. 2. When $\|e_i(t)\|$ reaches the upper limit, the event is triggered, and $\|e_i(t)\|$ is updated with the actual value observed by the event observer and cleared to zero. Accordingly, $\|e_i(t)\|$ gradually increases until the next event-triggered instant arrives, and the upper limit gradually converges to zero. Therefore, during the interval between the triggering instants of the two events, there is no communication between the DGs, and only the upper limit of the trigger time is obtained through the trigger function. The trigger function design uses only local and adjacent state information.

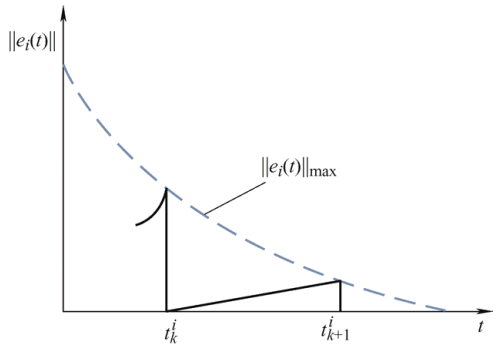

Fig. 2 Event-triggered time

The finite-time event-triggered function for secondary frequency control and active power-sharing

is designed as follows: Combining Eqs. (26) and (27), Eq. (25) can be rewritten as follows

$$\begin{cases} u_{\omega i} = -\beta_{\omega i} sign\left\{\left\{\sum_{j\in N_i} a_{ij}\left[\left(\omega_i-\omega_j\right)+\left(e_{\omega i}-e_{\omega j}\right)\right]+ \right.\right. \\ \left.\left. b_i\left(\omega_i+e_{\omega i}-\omega_{ref}\right)\right\}^{\alpha_{\omega i}}\right\} \\ u_{Pi} = -\beta_{Pi} sign\left\{\left\{\sum_{j\in N_i} a_{ij}\left[\begin{matrix}\left(K_{Pi}P_i-K_{Pj}P_j\right)+ \\ \left(e_{Pi}-e_{Pj}\right)\end{matrix}\right]\right\}^{\alpha_{Pi}}\right\} \end{cases} \tag{28}$$

By defining the frequency error, $\varepsilon_{\omega i}(t)=\omega_i(t)-\omega_{ref}$, Eq. (28) can be written as follows

$$\begin{cases} u_{\omega i} = -\beta_{\omega i} sign\left\{\left\{\sum_{j\in N_i} a_{ij}\left[\left(b_i/a_{ij}+1\right)\varepsilon_{\omega i}-\varepsilon_{\omega j}\right]+ \right.\right. \\ \left.\left. \sum_{j\in N_i} a_{ij}\left[\left(b_i/a_{ij}+1\right)\varepsilon_{\omega i}-\varepsilon_{\omega j}\right]\right\}^{\alpha_{\omega i}}\right\} \\ u_{Pi} = -\beta_{Pi} sign\left\{\left\{\sum_{j\in N_i} a_{ij}\left[\begin{matrix}\left(K_{Pi}P_i-K_{Pj}P_j\right)+ \\ \left(e_{Pi}-e_{Pj}\right)\end{matrix}\right]\right\}^{\alpha_{Pi}}\right\} \end{cases} \tag{29}$$

where the frequency threshold $y_{\omega i}(t)$, observation error $E_{\omega i}(t)$, active power threshold $y_{Pi}(t)$, and observation error $E_{Pi}(t)$ are introduced and defined as follows

$$\begin{cases} y_{\omega i}(t) = -\sum_{j\in N_i} a_{ij}\left[\left(b_i/a_{ij}+1\right)\varepsilon_{\omega i}-\varepsilon_{\omega j}\right] \\ E_{\omega i}(t) = -\sum_{j\in N_i} a_{ij}\left[\left(b_i/a_{ij}+1\right)e_{\omega i}-e_{\omega j}\right] \end{cases} \tag{30}$$

$$\begin{cases} y_{Pi}(t) = -\sum_{j\in N_i} a_{ij}(K_{Pi}P_i-K_{Pj}P_j) \\ E_{Pi}(t) = -\sum_{j\in N_i} a_{ij}(e_{Pi}-e_{Pj}) \end{cases} \tag{31}$$

To enable the system to achieve frequency restoration control and active power share in proportion within finite time, the event-triggered function designed is given by Eq. (32).

$$\begin{cases} f_{\omega i}(E_{\omega i}, y_{\omega i}) = E_{\omega i}(t) - k_{\omega i} y_{\omega i}(t) \\ f_{Pi}(E_{Pi}, y_{Pi}) = E_{Pi}(t) - k_{Pi} y_{Pi}(t) \end{cases} \tag{32}$$

where $k_{\omega i}$, k_{Pi} denote the frequency threshold coefficient and active power threshold coefficient, respectively, and $k_{\omega i}>0$, $k_{Pi}>0$.

3.2 Voltage secondary controller design

A voltage secondary controller was designed to restore the output frequency of each DG to its rated value. Using the input-output feedback linearization method, the dynamic system obtained by taking the derivative of Eq. (1) is

$$\dot{v}_i(t) = \dot{v}_0 - K_{Qi}\dot{Q}_i = u_{vi}(t) \tag{33}$$

where $u_{vi}(t)$ is the secondary voltage controller of DG_i.

According to the finite-time consensus algorithm shown in Eq. (10), the secondary controller u_{vi} designed for the voltage control input is

$$u_{vi} = -\beta_{vi} sign\left\{\left[\sum_{j\in N_i} a_{ij}\left(v_i-v_j\right)+b_i\left(v_i-v_{ref}\right)\right]^{\alpha_{vi}}\right\} \tag{34}$$

To reduce the dependence of the DGs units on the communication network, an event-triggered method is adopted, and Eq. (34) is transformed into the following form

$$u_{vi} = -\beta_{vi} sign\left\{\left[\sum_{j\in N_i} a_{ij}\left(\hat{v}_i-\hat{v}_j\right)+b_i\left(\hat{v}_i-v_{ref}\right)\right]^{\alpha_{vi}}\right\} \tag{35}$$

where ^ denotes the observed value of the corresponding variable, expressed as follows

$$\hat{v}_i(t) = v_i(t_{l_{vi}}) \tag{36}$$

where l_{vi} represents the l-th event triggered by the voltage controller of DG_i. To determine the triggering instants of the event, the voltage observation error $e_{vi}(t)$ is defined as

$$e_{vi}(t) = v_i(t_{l_{vi}}) - v_i(t) \tag{37}$$

The distributed finite-time event-triggered function for secondary voltage control is designed as follows: By combining Eqs. (36) and (37), Eq. (35) can be rewritten as follows

$$u_{vi} = -\beta_{vi} sign\left\{\left\{\sum_{j\in N_i} a_{ij}\left[\left(v_i-v_j\right)+\left(e_{vi}-e_{vj}\right)\right]+ \right.\right.$$
$$\left.\left. b_i\left(v_i+e_{vi}-v_{ref}\right)\right\}^{\alpha_{vi}}\right\} \tag{38}$$

By defining the voltage error, $\varepsilon_{vi}(t)=v_i(t)-v_{ref}$, Eq. (38) can be expressed as

$$u_{vi} = -\beta_{vi} sign\left\{\left\{\sum_{j\in N_i} a_{ij}\left[\left(b_i/a_{ij}+1\right)\varepsilon_{vi}-\varepsilon_{vj}\right]+ \right.\right.$$
$$\left.\left. \sum_{j\in N_i} a_{ij}\left[\left(b_i/a_{ij}+1\right)\varepsilon_{vi}-\varepsilon_{vj}\right]\right\}^{\alpha_{vi}}\right\} \tag{39}$$

The voltage threshold $y_{vi}(t)$ and observation error

$E_{vi}(t)$ are introduced and defined in the equations.

$$\begin{cases} y_{vi}(t) = -\sum_{j\in N_i} a_{ij}\left[\left(b_i / a_{ij} + 1\right)\varepsilon_{vi} - \varepsilon_{vj}\right] \\ E_{vi}(t) = -\sum_{j\in N_i} a_{ij}\left[\left(b_i / a_{ij} + 1\right)e_{vi} - e_{vj}\right] \end{cases} \tag{40}$$

To enable the system to achieve voltage restoration control in a finite time, an event-triggered function is designed, as shown in Eq. (41).

$$f_{vi}(E_{vi}, y_{vi}) = E_{vi}(t) - k_{vi}y_{vi}(t) \tag{41}$$

where k_{vi} is the voltage threshold coefficient, and $k_{vi} > 0$.

Based on Eqs. (25) and (35), the finite-time event-triggered control block diagram is as shown in Fig. 3.

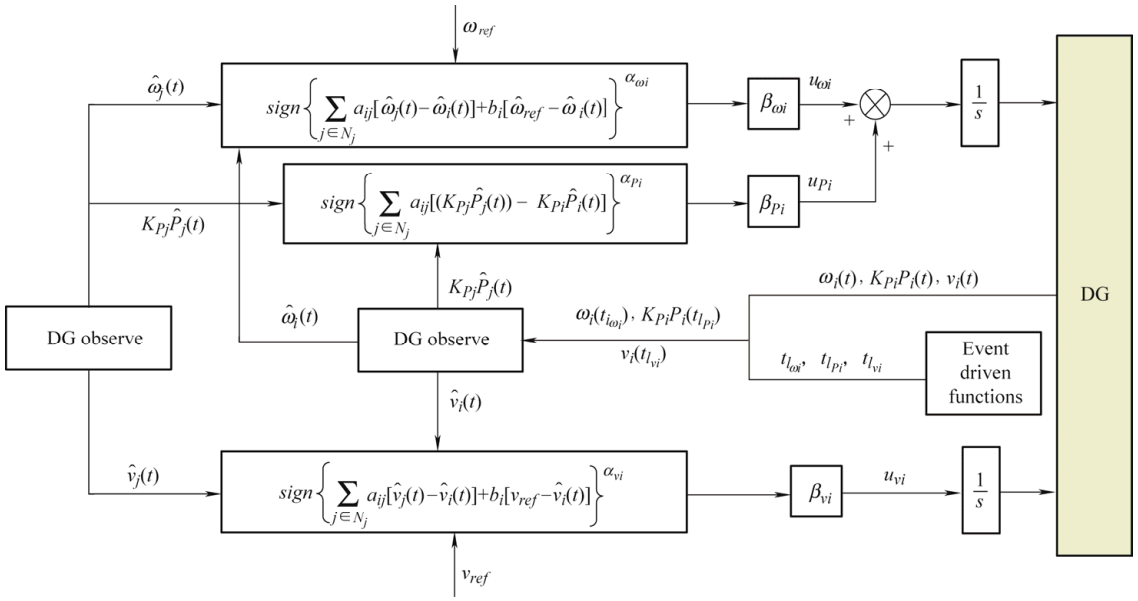

Fig. 3 Block diagram of the distributed finite-time event-triggered control method

In Fig. 3, the DG_i controller contains DG_i and DG_j observers, and only outputs the actual state values when DG_j events are triggered. Simultaneously, DG_i is transmitted to its neighbors only when an event is triggered, significantly reducing the communication between agents.

4 Simulation analysis

To verify the effectiveness of the proposed control method, a microgrid system with five parallel 3 kW DGs was developed in Matlab/Simulink, and the communication topology is shown in Fig. 4 [30]. The parameters are listed in Tab. 1 and Tab. 2.

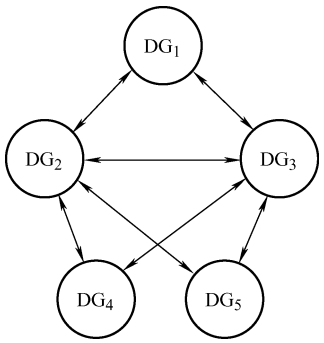

Fig. 4 DG communication topology

Tab. 1 Test results of samples

Parameter	DG_1&DG_2&DG_5	DG_3&DG_4
R_f/Ω	0.1	0.2
L_f/μH	13.5	9.5
C_f/μF	25	13
k_P	9.4×10^{-3}	12.5×10^{-3}
K_q	1.3×10^{-3}	1.5×10^{-3}
K_v	6	6
k_ω	4	4
Load/Ω	400	400

Tab. 2 Line parameters of microgrid system

Parameter	Line1&3	Line2	Line4	Line5
R_i/Ω	0.51	0.23	0.51	0.35
L_i/μH	1.05	0.318	1.05	0.7

According to communication topology and graph theory, the adjacency matrix $\boldsymbol{A}$, degree matrix $\boldsymbol{D}$, and Laplace matrix $\boldsymbol{L}$ are obtained.

$$\boldsymbol{A} = \begin{bmatrix} 0 & 1 & 1 & 0 & 0 \\ 1 & 0 & 1 & 1 & 1 \\ 1 & 1 & 0 & 1 & 1 \\ 0 & 1 & 1 & 0 & 0 \\ 0 & 1 & 1 & 0 & 0 \end{bmatrix} \quad \boldsymbol{D} = \begin{bmatrix} 2 & 0 & 0 & 0 & 0 \\ 0 & 4 & 0 & 0 & 0 \\ 0 & 0 & 4 & 0 & 0 \\ 0 & 0 & 0 & 2 & 0 \\ 0 & 0 & 0 & 0 & 2 \end{bmatrix} \tag{42}$$

$$\boldsymbol{L}=\begin{bmatrix} 2 & -1 & -1 & 0 & 0 \\ -1 & 4 & -1 & -1 & -1 \\ -1 & -1 & 4 & -1 & -1 \\ 0 & -1 & -1 & 2 & 0 \\ 0 & -1 & -1 & 0 & 2 \end{bmatrix} \tag{43}$$

To verify the dynamic performance of the control system, only the primary droop control was added before $t=2$ s; finite-time event-triggered consensus control was added at $t=2$ s, and load changes were added at $t=6$ s and $t=10$ s.

4.1 System dynamic performance simulation analysis

The dynamic performance of the finite-time event-triggered consensus coordination control method is shown in Fig. 5.

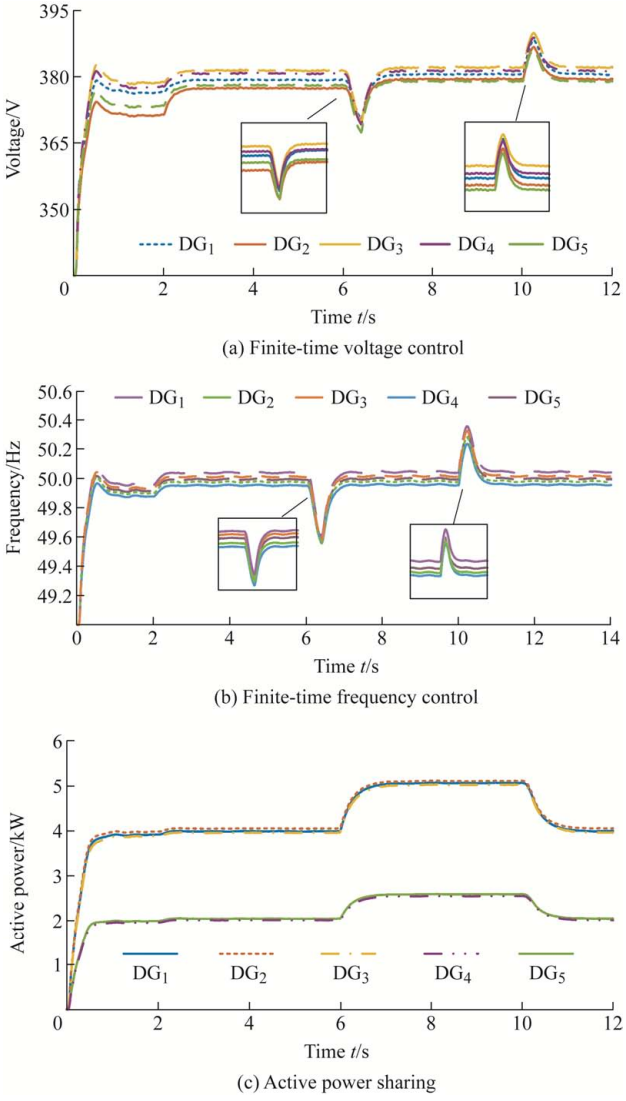

(a) Finite-time voltage control

(b) Finite-time frequency control

(c) Active power sharing

Fig. 5 System dynamic performance analysis

From Figs. 5a and 5b, before $t=2$ s, using only the droop control method, the voltage and frequency range from 368 V to 375 V and from 49.8 Hz to 50 Hz, respectively; however, there are deviations from the rated value. At $t=2$ s, after using the finite-time event-triggered consensus control, the frequency gradually rises to the rated value, and the output voltage rises to 380 V. To analyze the dynamic performance of the controller, a resistive load of 400 Ω was cut in at $t=6$ s, and the voltage and frequency decreased simultaneously; When $t=10$ s, the load was cut off, and the voltage and frequency increased accordingly but quickly stabilized to the rated value. This indicates that the finite-time event-triggered consensus coordination control method can quickly eliminate the voltage and frequency fluctuations caused by load changes. This shows that the system has good dynamic performance and robustness and can adapt to uncertain disturbances.

Fig. 5c shows the active power sharing waveform obtained using the finite-time event-triggered consensus control method. As shown in Fig. 5c, following finite-time event-triggered consensus control, the active power can be shown precisely according to the DG capacity ratio of 2:1. To further analyze the problem of active power sharing under load change, at $t=6$ s, the 1.5 kW load is cut in; at $t=10$ s, the 1.5 kW load is cut off. It can be observed that the active power can still maintain the ratio for distribution under the load cut in, which reflects the good dynamic performance of the proposed control method.

According to the event-triggered time generation process shown in Fig. 2 and the designed event-triggered conditions, the system voltage, frequency event-triggered instants, and active power proportional share event-triggered instants using finite-time event-triggered consensus coordination control are shown in Fig. 6.

As shown in Fig. 6, the event-triggered numbers are limited to finite times. Communication between controllers is performed when events are triggered, which means that the communication between controllers is discrete. Using the finite-time event-triggered consensus coordination control method effectively reduces the communication burden between the controllers.

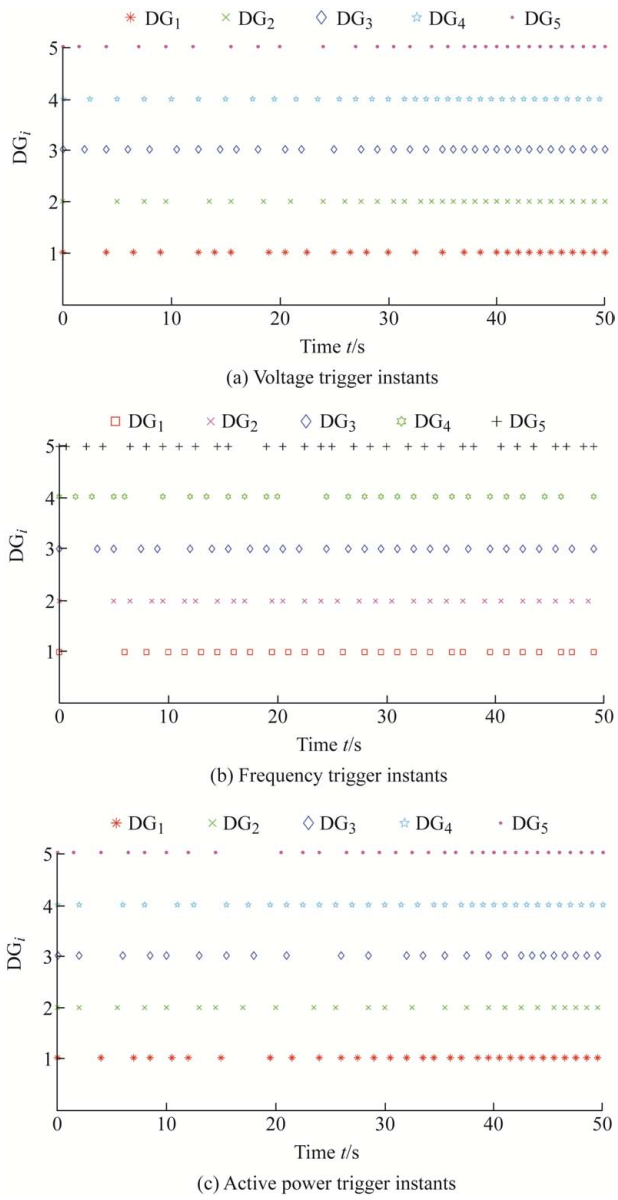

Fig. 6 Event-triggered instants

4.2 Comparison of system voltage and frequency dynamic response

A comparison of the system voltage and frequency dynamic responses between the finite-time event-triggered consensus coordination control method, time-triggered consensus control method, and event-triggered consensus control method are shown in Fig. 7.

As shown in Fig. 7, the finite-time event-triggered consensus coordination control, time-triggered consensus control, and event-triggered consensus control methods stabilize the output voltage and system frequency at the rated values. In the case of load cut in, the finite-time event-triggered consensus coordination control method has a faster response speed and can quickly stabilize the voltage and frequency at the rated values within a finite time. The finite-time event-triggered consensus coordination control method converges at $t = 6.2$ s, and the event-triggered control method and time-triggered control method converge at $t = 7$ s and $t = 7.5$ s, respectively. It can be observed that the proposed method has better dynamic performance. The voltage and frequency fluctuations are also smaller. Compared with the time-triggered and event-triggered control methods, the voltage deviation of the finite-time event-triggered consensus coordination control method is reduced by 5.8 V and 4.3 V, respectively. The frequency deviation is reduced using 0.09 Hz and 0.05 Hz, respectively. Therefore, the finite-time event-triggered consensus coordination control method exhibits better dynamic performance.

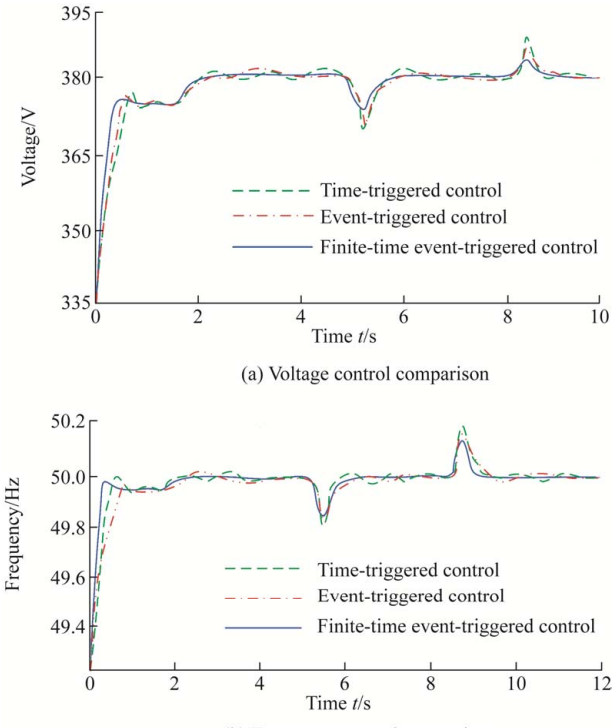

Fig. 7 Comparison of voltage and frequency controls

A comparison of the number of finite-time event-triggered consensus control communications, time-triggered consensus control communications, and event-triggered consensus control is shown in Fig. 8.

As shown in Fig. 8, under the condition of ensuring system voltage and frequency stability, the communication numbers for the finite-time event-triggered consensus coordination control method are lower than that of time-triggered control. However,

because the finite-time event-triggered consensus coordination control method considers the control performance and rate of convergence, the communication numbers are greater than those of the event-triggered control method. The finite-time event-triggered consensus coordination control method can ensure that the voltage and frequency are stable at the rated values. Fewer communication numbers can effectively reduce the network bandwidth required for communication.

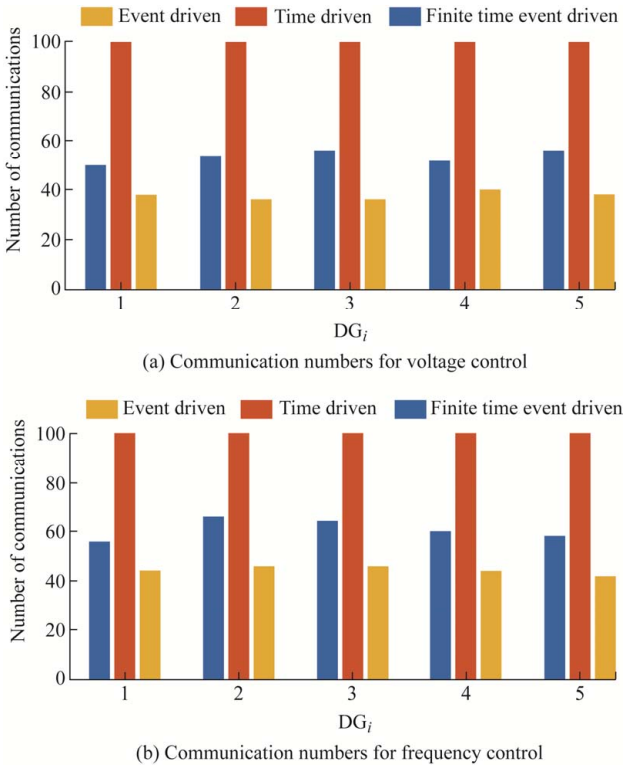

Fig. 8 Comparison of communication numbers

A comparison diagram of the control instants for the finite-time event-triggered consensus coordination control method and time-triggered consensus control method is shown in Fig. 9.

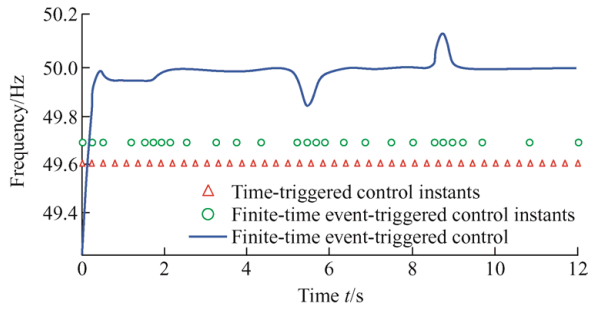

Fig. 9 Comparison diagram of control instants

Taking DG_3 as an example, it can be observed from Fig. 9 that when using the time-triggered consensus control method, the controller triggers at equal intervals. Even though the system is already in a stable state, the controller still needs to trigger, resulting in an excessive network bandwidth burden.

When using the finite-time event-triggered consensus coordination control method, the controller triggers densely only when a load is cut in. When the system is in a stable state, the frequency of the controller trigger is significantly reduced, effectively saving controller resources.

5 Conclusions

A consensus coordination control method based on a finite-time event-triggered consensus algorithm was proposed to address the problems of high sampling rate, high number of controller updates, and voltage and frequency deviations from rated values caused by droop control in the networked control of microgrid systems. Voltage and frequency secondary controllers were designed based on finite-time event-triggered consensus algorithms. The simulation analysis showed that the proposed finite-time event-triggered consensus coordination control method can quickly restore the voltage and frequency deviations generated by the primary droop control to the rated value. It can reduce the number of communication transmissions between the controllers and the communication bandwidth of the system, thereby saving communication resources. The finite-time event-triggered consensus coordination control method avoided the Zeno phenomenon. Moreover, when the load changes, it can quickly restore the voltage and frequency to stabilize at the rated value and realize accurate active power sharing. The system exhibited good dynamic performance.

Currently, research on event-triggered control primarily focuses on theoretical applications and experimental analyses. Further research is needed to apply this theory in engineering practice. In addition, as a crucial component of smart energy systems, it is necessary to conduct in-depth research on consensus coordination control methods of microgrid systems under network attacks.

References

[1] E Du, N Zhang, B M Hodge, et al. The role of concentrating solar power toward high renewable energy penetrated power systems. *IEEE Transactions on Power*

Systems, 2018, 33(6): 6630-6641.

[2] B Sahoo, S K Routray, P K Rout. AC, DC, and hybrid control strategies for smart microgrid application: A review. *International Transactions on Electrical Energy Systems*, 2021, 31(1): e12683.

[3] S Jadidi, H Badihi, Y Zhang. A review on operation, control and protection of smart microgrid. *IEEE 2nd International Conference on Renewable Energy and Power Engineering (REPE)*. Toronto, ON, Canada. IEEE, 2019: 100-104.

[4] S Aslam, H Herodotou, S M Mohsin, et al. A survey on deep learning methods for power load and renewable energy forecasting in smart microgrids. *Renewable and Sustainable Energy Reviews*, 2021, 144: 621-644.

[5] J M Guerrero, M Chandorkar, T L Lee, et al. Advanced control architectures for intelligent microgrids—part i: Decentralized and hierarchical control. *IEEE Transactions on Industrial Electronics*, 2013, 60(4): 1254-1262.

[6] J M Guerrero, J C Vasquez, J Matas, et al. Hierarchical control of droop-controlled AC and DC microgrids: A general approach toward standardization. *IEEE Transactions on Industrial Electronics*, 2011, 58(1): 158-172.

[7] L Ding, Q L Han, X M Zhang. Distributed secondary control for active power sharing and frequency regulation in islanded microgrids using an event-triggered communication mechanism. *IEEE Transactions on Industrial Informatics*, 2019, 15(7): 3910-3922.

[8] A Kaur, J Kaushal, P Basak. A review on microgrid central controller. *Renewable and Sustainable Energy Reviews*, 2016, 55: 338-345.

[9] A Bidram, A Davoudi, F L Lewis, et al. Distributed cooperative secondary control of microgrids using feedback linearization. *IEEE Transactions on Power Systems*, 2013, 28(3): 3462-3470.

[10] W Zhang, H Zhang, N Zhi. Energy management optimization strategy of DC microgrid based on consensus algorithm considering generation economy. *Energy Reports*, 2023, 9: 683-691.

[11] X Meng, T Chen. Event based agreement protocols for multi-agent networks. *Automatica*, 2013, 49(7): 2125-2132.

[12] Y Chu, S Xu, Y Li, et al. Consensus for multi-agent systems with distributed adaptive control and an event-triggered communication strategy. *IET Control Theory and Applications*, 2016, 10(13): 1547-1555.

[13] S Sahoo, S Mishra. An adaptive event-triggered communication-based distributed secondary control for DC microgrids. *IEEE Transactions on Smart Grid*, 2018, 9(6): 6674-6683.

[14] D Pullaguram, S Mishra, N Senroy. Event-triggered communication based distributed control scheme for DC microgrid. *IEEE Transactions on Power Systems*, 2018, 33(5): 5583-5593.

[15] B Fan, J Peng, Q Yang, et al. Distributed periodic event-triggered algorithm for current sharing and voltage regulation in DC microgrids. *IEEE Transactions on Smart Grid*, 2019, 11(1): 577-589.

[16] F Yuan, G Hu, M Egerstedt. Distributed reactive power sharing control for microgrids with event-triggered communication. *IEEE Transactions on Control Systems Technology*, 2016, 25(1): 118-128.

[17] C Meng, X Xiao, J M Guerrero. Secondary restoration control of islanded microgrids with a decentralized event-triggered strategy. *IEEE Transactions on Industrial Informatics*, 2018, 14(9): 3870-3880.

[18] B Abdolmaleki, A R Seifi, M M Arefi, et al. Event-triggered voltage control of inverter-based microgrids. *2018 9th Annual Power Electronics, Drives Systems and Technologies Conference (PEDSTC)*, 2018: 522-528.

[19] B Abdolmaleki, Q Shafiee, A R Seifi, et al. A zeno-free event-triggered secondary control for AC microgrids. *IEEE Transactions on Smart Grid*, 2020, 11(3): 1905-1916.

[20] L Ding, Q L Han, X M Zhang. Distributed secondary control for active power sharing and frequency regulation in islanded microgrids using an event-triggered communication mechanism. *IEEE Transactions on Industrial Informatics*, 2019, 15(7): 3910-3922.

[21] X Jin, W Du, L H Wang, et al. Twisting-based finite-time consensus for euler-lagrange systems with an event-triggered strategy. *IEEE Transactions on Network Science and Engineering*, 2020, 7(3): 1007-1018.

[22] Y Zhao, Y F Liu, G H Wen, et al. Edge-based finite-time protocol analysis with final consensus value and settling time estimations. *IEEE Transactions on Cybernetics*, 2020, 50(4): 1450-1459.

[23] J L Wang, Q Wang, H N Wu, et al. Finite-time consensus and finite-time H∞ consensus of multi-agent systems under directed topology. *IEEE Transactions on Network Science and Engineering*, 2020, 7(3): 1619-1632.

[24] X J Ma, F Li, M Zhao, et al. Distributed finite-time consensus cooperative secondary control of microgrid. *Electric Machines and Control*, 2021, 25(2): 45-53.

[25] F Guo, C Wen, J Mao, et al. Distributed secondary voltage and frequency restoration control of droop-controlled inverter-based microgrids. *IEEE Transactions on Industrial Electronics*, 2015, 62(7): 4355-4364.

[26] T Zhao, Z Ding. Distributed finite-time optimal resource management for microgrids based on multi-agent framework. *IEEE Transactions on Industrial Electronics*, 2018, 65(8): 6571-6580.

[27] Z Wang, H Li, H He, et al. Robust distributed finite-time secondary frequency control of islanded ac microgrids with event-triggered mechanism. *2023 IEEE Power & Energy Society Innovative Smart Grid Technologies Conference (ISGT)*, January 16-19, 2023, Washington, DC, USA. IEEE, 2023: 1-5.

[28] J Choi, A Bidram. Distributed finite-time event-triggered current sharing and voltage control of DC microgrids. *International Journal of Electrical Power & Energy Systems*, 2023, 151: 109142.

[29] J P Zhou, J Zhang, D J Mao, et al. Distributed finite-time event-triggered secondary coordinated control of islanded microgrids. *Electric Power Automation Equipment*, 2021, 41(11): 127-132.

[30] C Su, Z J Wu, H Y Li, et al. Distributed secondary control strategy and its communication topology optimization for islanded microgrid. *Transactions of China Electrotechnical Society*, 2017, 32(6): 209-219.

Lizhen Wu received the M.S. degree in the Control Theory and Control Engineering from Lanzhou University of Technology, Gansu, China, in 2004, and the Ph.D. degree in Control Theory and Control Engineering from Lanzhou University of Technology in 2017, respectively. She is studying in power system and its automation in National Active Distribution Network Technology Research Center, Beijing Jiaotong University, Beijing, China, in 2015. Currently, she is an Associate Professor/Master Supervisor at College of Electrical and Information Engineering, Lanzhou University of Technology, where she teaches courses on power electronics, control theory and renewable energy systems. Her interests include distributed generation and microgrids, micro-energy grid coordination control, power quality control, artificial intelligence and data-driven theory for smart grid, networked control theory and its application.

Heng Yang received the B.Eng. degree in Automation from Shanghai University of Electric Power, Shanghai, China. He is currently a Master degree candidate at the Lanzhou University of Technology, Gansu, China, in 2022. His interests include coordination control of microgrid.

Jianping Wei received the B.Eng. degree in Electrical Engineering from Lanzhou University of Technology, Gansu, China. He is currently a Master degree candidate at the Lanzhou University of Technology, Gansu, China, in 2021. His interests include coordination control of distributed generation and micro-energy system.

Wendong Jiang received the B.Eng. degree in in Electrical Engineering from Lanzhou University of Technology, Gansu, China. He is currently working at State Grid Yinchuan Branch, Yinchuan, China, in 2023. His interests include distributed generation and microgrid coordination control.